RSC Advances

PAPER

View Article Online
View Journal | View Issue

Cite this: *RSC Adv.*, 2014, **4**, 50226

Influence of method of preparation on the activity of La–Ni–Ce mixed oxide catalysts for dry reforming of methane†

T. V. Sagar,[a] N. Sreelatha,[a] G. Hanmant,[b] M. Surendar,[a] N. Lingaiah,[a] K. S. Rama Rao,[a] C. V. V. Satyanarayana,[b] I. A. K. Reddy[c] and P. S. Sai Prasad*[a]

Received 14th July 2014
Accepted 29th September 2014

DOI: 10.1039/c4ra07098d

www.rsc.org/advances

$La–Ni_x–Ce_{1-x}$ mixed oxide catalysts were prepared by a sol–gel method varying the Ni composition ($0 \leq x \leq 1$). The catalysts were characterized by X-ray diffraction (XRD), inductively coupled plasma optical emission spectroscopy (ICP-OES), BET surface area, X-ray photoelectron spectroscopy (XPS), temperature-programmed reduction (TPR), H_2 chemisorption and Fourier transform infrared spectroscopy (FT-IR) techniques. CO_2 reforming of methane was carried out at atmospheric pressure and 800 °C, maintaining a reactant $CO_2/CH_4/N_2$ ratio of 80/80/80 (total flow rate = 240 ml min^{-1}, GHSV of 28 800 h^{-1}). The catalysts offered higher activity even at lower Ni compositions. $LaNi_{0.4}Ce_{0.6}O_3$. showed the highest conversion of CH_4 and CO_2. The H_2/CO ratio in the syngas was stable at 0.85 ± 0.02. The performance of the sol–gel catalysts was compared with that of the hydrothermally prepared catalysts, reported earlier. High surface area and better Ni dispersion were found to be the reasons for superior activity of the sol–gel catalysts.

1. Introduction

As methane and carbon dioxide are recognized as the major contributors to global warming, their emissions into the atmosphere have to be restricted. For carbon dioxide emission control, the carbon capture and sequestration (CCS) technology is vigorously pursued. However, carbon dioxide is nowadays viewed as a cheap raw material for chemical synthesis rather than its expensive capture and storage. Catalytic carbon dioxide reforming or dry reforming of methane is found to be an important method for this purpose not only for regulating the gas emissions but also to generate useful syngas that can produce oxygenated products *via* Fisher–Tropsch synthesis.[1] Dry reforming is a highly endothermic reaction necessitating high reaction temperatures at which coke formation and sintering of catalysts become serious problems for smooth transformation of the reactants into products. Noble metal catalysts like Pt, Pd, Rh and Ir have been explored for this purpose as they show better coke and sulfur resistance.[2,3] However, their limited availability and high cost make them less attractive for commercial applications. In this aspect, nickel based catalysts are technically and economically viable for the reforming reaction.[4] In order to prevent Ni from deactivation due to coke formation and sintering,[5] its insertion in a definite chemical structure like the ABO_3 type perovskite is often adopted. The perovskite $LaNiO_3$ is generally preferred as La affords thermal stability[6] and Ni provides catalytic activity. Modifications to this perovskite in the form of $LaNi_{1-x}M_xO_3$ (M = Mg, Cu, Rh, Ru, Co, Fe and Al)[7] and $LaNi_xM_{1-x}O_3$ (M = Al, Fe)[8,9] are also reported with $LaNi_{0.3}Al_{0.7}O_3$ suggested as the best system.[8]

The advantages of inclusion of Ce in the mixed oxide system have been extensively studied by many researchers. The enhancement in catalytic behavior by presence of CeO_2 was attributed to its unique structural and redox properties.[10] In the reforming reaction, the rate is controlled by the interaction of adsorbed methane or surface hydrocarbon species with lattice oxygen in CeO_2, as it is the slow reaction step. This step is followed by a rapid gas–solid reaction between reactant CO_2 and the reduced support Ce_2O_3 to regenerate the lattice oxygen. Besides, due to its high oxygen storage capacity CeO_2 could enhance the activity of the perovskite catalysts[11,12] and as a promoter increases Ni dispersion, which enables decrease in the coke formation on the Ni surface.[13] $La_{1-x}Ce_xNiO_3$ prepared by substitution of Ce in place of La was studied by Qi *et al.*[14] leaving the Ni composition constant. In a recent publication,[15] we have reported that catalysts prepared by hydrothermal method and varying Ni and Ce composition, keeping La constant, offer better activity. Recently, Ni–Ce oxide solid solution has shown much promise in its methane partial oxidation activity.[16] Xu *et al.*[17] also studied autothermal reforming of

[a]*Inorganic and Physical Chemistry Division, CSIR – Indian Institute of Chemical Technology, Uppal Road, Hyderabad – 500 607, India. E-mail: saiprasad@iict.res.in; Fax: +91 40 27160921; Tel: +91-40-2719 3163*

[b]*CSIR – National Chemical Laboratory, Pune-411008, India*

[c]*National Institute of Technology, Warangal-506004, India*

† Electronic supplementary information (ESI) available: XPS figures of Ni 2p, O 1s and C 1s of $La–Ni_x–Ce_{1-x}$ mixed oxide catalysts. See DOI: 10.1039/c4ra07098d

methane on Ce–Ni oxide catalysts. Dry reforming of methane has not been reported on Ni–Ce oxide solid solution or the solid solution containing mixed oxide catalysts.

The aim of the present work is to examine the influence of method of preparation on the activity of the catalyst during methane dry reforming. $LaNi_xCe_{1-x}O_3$ catalysts were prepared by sol–gel method and their activity was compared with those prepared by hydrothermal method. The advantages of the sol–gel method over the hydrothermal method were brought forward.

2. Experimental

2.1 Catalyst preparation

The sol–gel method similar to that reported in the literature[9] was adopted for the synthesis of the La–Ni_x–Ce_{1-x} oxide catalysts with $0 \leq x \leq 1$. Required amounts of $La(NO_3)_3 \cdot 6H_2O$ (Fluka), $Ni(NO_3)_2 \cdot 6H_2O$ (SD fine) and $Ce(NO_3)_3 \cdot 9H_2O$ (SD fine) were separately dissolved in known quantities of hot propionic acid. After mixing and stirring under reflux for 24 h, the resin like material obtained was dried at reduced pressure and calcined at 800 °C with a temperature ramping of 2 °C min^{-1}. The quantities of nitrate salts were selected in such a way that the finished catalysts contained their Ni content with $x = 0.2$, 0.3, 0.4, 0.6 and 0.8. A sample with $x = 1.0$ (*i.e.*, La–Ni oxide sample without Ce) was also prepared for the sake of comparison.

2.2 Characterization studies

The XRD patterns of the catalysts were obtained on an Ultima-IV diffractometer (M s^{-1}. Rigaku Corporation, Japan) using nickel-filtered Cu Kα radiation ($\lambda = 1.54$ Å). The measurements were recorded in steps of 0.045° with count time of 0.5 s in 2θ range of 10 to 80°. Identification of the crystalline phases was made with the help of JCPDS files. BET surface areas were determined by N_2 adsorption on a SMART SORB 92/93 instrument (M s^{-1}. SMART Instruments, India). Prior to BET measurement, the samples were dried at 150 °C for 2 h. The chemical analysis of the samples was carried out by inductively coupled plasma optical emission spectroscopy (ICP-OES) using a Varian 725ES instrument. TPR studies were performed using a home-made apparatus. Catalyst samples (50 mg), taken in a quartz reactor, were reduced with 10% H_2–Ar gas mixture flowing at a flow rate of 30 ml min^{-1} and with heating rate of 5 °C min^{-1} up to 900 °C. Before the TPR run, the catalysts were pretreated in argon at 300 °C for 2 h. The hydrogen consumption was monitored using thermal conductivity detector of a gas chromatograph (Varian, 8301). FT-IR spectra were obtained on a Perkin Elmer (Spectrum GX, USA) instrument, using KBr pellet method. XPS measurements were made on a KRATOS AXIS 165 instrument. The non-monochromatized Al-Kα X-ray source ($h\nu = 1486.6$ eV) was operated at 12.5 kV and 16 mA. Before acquisition of the data the sample was out-gassed for about 3 h at 100 °C under a pressure of 1.0 x 10^{-2} torr to minimize surface contamination. The XPS instrument was calibrated using Au as a standard material. For energy calibration, the carbon 1s photoelectron line (285 eV) was used. Charge neutralization of 2 eV was used to balance the charge up of the sample. The spectra were deconvoluted using Sun Solaris based Vision-2 curve resolver. The location and the full width at half maximum (FWHM) value for the species were first determined using the spectrum of pure sample. The location and FWHM of products, which were not obtained as pure species were adjusted until the best fit was obtained. Symmetric Gaussian shapes were used in all cases. Binding energies for identical samples were, in general reproducible within ±0.1 eV. H_2 Chemisorptions studies were performed using an Autosorb iQ apparatus. Catalyst samples (30 mg), taken in a quartz reactor, were first reduced in H_2 gas at a flow rate of 60 ml min^{-1} and with a heating rate of 10 °C min^{-1} up to 600 °C. They were then cooled in He flow to room temperature. Hydrogen gas was then introduced in pulses and the adsorption uptake was analyzed using a TCD. The coke content of the used catalysts was determined in CHNS analyzer (ElementaV, Germany).

2.3 Catalytic activity test

The evaluation of catalysts was performed in a fixed-bed quartz micro reactor (i.d. 12 mm) under atmospheric pressure by passing a mixture of CO_2, CH_4 and N_2 at a $CO_2/CH_4/N_2$ ratio of 80/80/80 (total flow rate = 240 ml min^{-1}, GHSV of 28 800 h^{-1}). The activity tests were carried out using 0.5 cm^3 (~0.8 g) of catalyst (18/25 BSS mesh) diluted with 50% of the ceramic beads. Prior to the activity measurements, the samples were reduced *in situ* under 60% H_2–N_2 gas mixtures at 600 °C for 6 h. The data were analyzed online on a Chemito 8610 gas chromatograph equipped with a carbosphere column using Argon as a carrier gas and a TCD detector. After attaining the required temperature, the reaction was allowed to attain steady-state for a period of 1 h. Subsequently, the product analysis was carried out three times with an interval of 30 min. The values provided here are the average values. The accuracy was within ±5%.

3. Results and discussion

3.1 Surface area & X-ray diffraction

Table 1 illustrates the specific surface areas of the catalysts. The surface area is seen to increase initially in catalysts up to $x = 0.3$ followed by a decreasing trend. The decrease is more perceptible beyond $x = 0.6$. The specific surface area values are much

Table 1 Specific surface area (SSA) and FT-IR bands of catalyst systems

		FT-IR (cm^{-1})		
Catalyst	SSA (m^2 g^{-1})	δ_s (CH_3)	δ_{as} (CH_3) & ν_3 (NO)	ν_3 (NO)
$LaNi_{0.8}Ce_{0.2}O_3$	1.39	1464	1379	—
$LaNi_{0.6}Ce_{0.4}O_3$	9.29	1464	1379	850
$LaNi_{0.4}Ce_{0.6}O_3$	10.16	1471	1369	853
$LaNi_{0.3}Ce_{0.7}O_3$	11.67	1471	1369	850
$LaNi_{0.2}Ce_{0.8}O_3$	6.91	—	1376	858

higher than the catalysts prepared by the hydrothermal method (which varied between 0.4 to 4.1 $m^2\ g^{-1}$). Table 2 provides the experimental and estimated compositions of the sol–gel catalysts, which agreed very closely. The XRD patterns of the catalysts, including $LaNiO_3$ perovskite, are displayed in Fig. 1. At low x values, peaks due to La_2O_3 (2θ = 27.5, 31.9, 45.6 and 54.08°) only are found. A coherent 2θ shift towards lower angle is evidenced with increase of x for the $LaNi_xCe_{1-x}$ mixed oxides. This observation is due to the dissolution of Ni^{2+} ions in the La_2O_3 lattice forming the $LaNiO_3$ perovskite, as seen in catalysts with higher values of x. The peaks at 23.6, 32.9, 47.3 and 58.9° (2θ) clearly reveal the presence of the typical rhombohedral phase of $LaNiO_3$ (JCPDS 34-1028) with higher intensity, particularly in catalysts with $x = 0.8$ and 1.0. A drastic decrease in the surface area (Table 1) in these samples also indicates the formation of crystalline perovskite. The NiO shows much diffused peaks in catalysts with low Ni content probably due to the presence of smaller sized particles, not being detected by XRD. Similarly, no peaks due to crystalline CeO_2 are observed, excepting its weak signals in catalysts with $x = 0.3$ and 0.4. The present XRD data, when compared with those of the results of Lima *et al.*,[18] reveal interesting points. In the case of catalysts reported by Lima *et al.*, with the substitution of La by Ce, there was the formation of $LaNiO_3$ and CeO_2 existed in a discrete crystalline phase.

On the other hand, in the present work when Ce is substituted for Ni, leaving lanthana constant, CeO_2 becomes amorphous and La_2O_3 crystallizes out. The appearance of La_2O_3 as a separate phase indicates greater interaction between Ni and Ce increasing the possibility of formation of Ni–Ce solid solution at low values of x, as reported in the literature,[19] though it is not clearly visible in the XRD patterns of the present samples. In order to verify the possibility of formation of the solid solution, samples containing Ce and Ni, with the same compositions as that of the mixed oxides were prepared separately and were examined by XRD analysis. These samples have indicated the formation of Ni–Ce oxide solid solution as evidenced by the decrease in the lattice parameter of CeO_2 from 5.430 to 5.416 Å (Fig. S1, ESI†). This lends credence to the hypothesis of the presence of Ni–Ce solid solution in the mixed oxide. Only at higher loadings crystalline Ni is noticed as a result of agglomeration. A comparison of the morphology of the present series of catalysts with those prepared by the hydrothermal method reveals an interesting observation. Even at low composition of Ni ($x = 0.2$ and 0.3), the hydrothermally prepared catalysts show the existence of $LaNiO_3$ in their XRD patterns; whereas such species are seen only at higher compositions in the sol–gel catalysts. The Ni dispersion, as calculated by H_2 chemisorptions also reveals higher values (18.65, 21.79 and 32.74%) for sol–gel samples with x = 0.2, 0.3 and 0.4, respectively compared to (10.34, 13.05 and 31.13%) for the hydrothermal catalysts of the same composition.

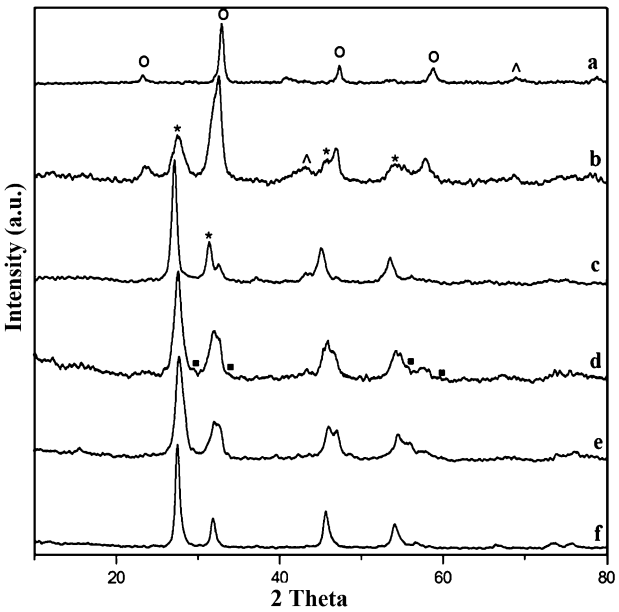

Fig. 1 XRD patterns of La–Ni_x–Ce_{1-x} mixed oxide catalysts. (a) $x = 1$; (b) $x = 0.8$; (c) $x = 0.6$; d) $x = 0.4$; (e) $x = 0.3$; and (f) $x = 0.2$. (*) La_2O_3, (O) $LaNiO_3$, (■) CeO_2, (^) NiO.

3.2 H_2-temperature programmed reduction

The TPR patterns of the $LaNi_xCe_{1-x}$ oxide catalysts are shown in Fig. 2. Usually, $LaNiO_3$ (inset) exhibits two peaks corresponding to $Ni^{3+} \rightarrow Ni^{2+}$ and $Ni^{2+} \rightarrow Ni^0$ reduction with the area ratio of second/first equaling 2, as reported in the literature.[20] It is interesting to note from the TPR profiles of the catalysts that the peak shapes and their temperature maxima have considerably varied with the Ni composition. At low x values, the catalysts essentially contain La_2O_3 as a discrete phase, which is not reducible. On the other hand, Ni and Ce oxides are the reducible species in the mixed oxides. In the case of Ni containing CeO_2 catalysts, Yonggang *et al.*[20] assigned the TPR peaks into α, β, γ and δ types. The α peak noticed at around 330 °C is due to the

Table 2 Elemental analysis of La–Ni_x–Ce_{1-x} catalytic systems

	Ni		Ce		La	
Catalysts	Theoretical	Experimental	Theoretical	Experimental	Theoretical	Experimental
$LaNi_{0.8}Ce_{0.2}O_3$	17.929	17.59	10.70	10.74	53.041	53.78
$LaNi_{0.6}Ce_{0.4}O_3$	12.659	11.36	20.14	20.54	49.436	52.17
$LaNi_{0.4}Ce_{0.6}O_3$	7.972	8.10	28.55	28.1	47.174	48.8
$LaNi_{0.3}Ce_{0.7}O_3$	5.818	5.79	32.41	33.2	45.905	46.01
$LaNi_{0.2}Ce_{0.8}O_3$	3.77	3.73	36.07	35.27	44.702	45.27

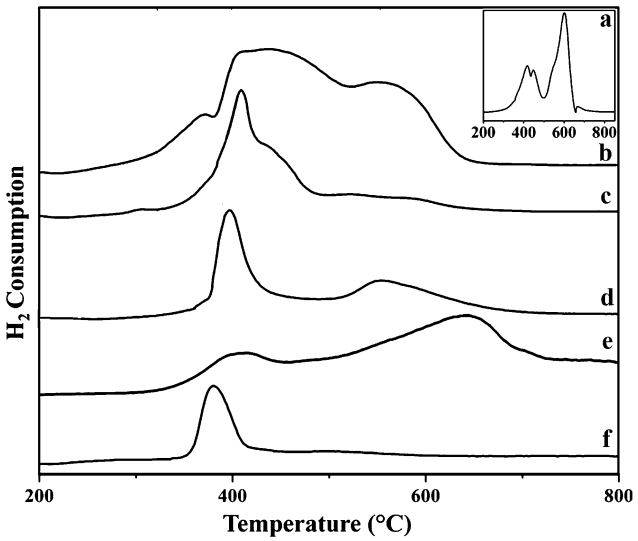

Fig. 2 TPR Profiles of La–Ni_x–Ce_{1-x} mixed oxide catalysts. (a) $x = 1$; (b) $x = 0.8$; (c) $x = 0.6$; (d) $x = 0.4$; (e) $x = 0.3$; and (f) $x = 0.2$.

reduction of the adsorbed oxygen on the Ni–Ce mixed oxide. The β peak appearing at 400 °C is specifically related to the reduction of NiO dispersed on ceria and the γ peak, normally observes at around 550 °C, and represents the reduction of NiO intimately in contact with CeO_2. The δ peak, on the other hand, is a result of the reduction of CeO_2 with its characteristic peak displayed beyond 800 °C (not seen in the present patterns). In the case of the present catalysts, the low temperature reduction peak (at temperatures <400 °C) is seen at higher Ni contents, whereas the β peak dominates in the catalysts indicating the availability of dispersed Ni species. The merging of γ peak with β can be due to agglomeration of NiO. The appearance of distinct peaks due to NiO in the XRD patterns of the catalysts with $x = 0.8$ and 0.6 also supports this phenomenon. It is also reported that the Ni species in Ni–Ce oxide solid solution are not easily reducible.[19]

Therefore, the peaks representing the reduction of Ni in the catalyst appear at higher temperature regions. This peak is distinguishable in catalysts with high Ni compositions. Thus, in support of the XRD results, the TPR information also confirms the presence of the perovskite ($LaNiO_3$) in the catalysts with high Ni loading and the existence of NiO in two forms, the agglomerated and the well dispersed species. Particularly, the catalyst with $x = 0.4$ displays combined characteristics of both the low and high Ni containing catalysts.

3.3 X-ray photoelectron spectroscopy

The core-level XPS profiles of La 3d of La–Ni_x–Ce_{1-x} mixed oxides are shown in Fig. 3. Due to the close similarity of binding energies of Ni $2p_{3/2}$ and La $3d_{3/2}$, it is difficult to distinguish between these two species.[21] On the other hand, the binding energies recorded at 853.7 and 836.8 eV fitted well with La $3d_{3/2}$ and $3d_{5/2}$ states, respectively. The most intense 853.7 eV peak overlaps with that of the Ni 2p peak due to Ni^{2+} in NiO (Fig. S2, ESI†).[16,22]

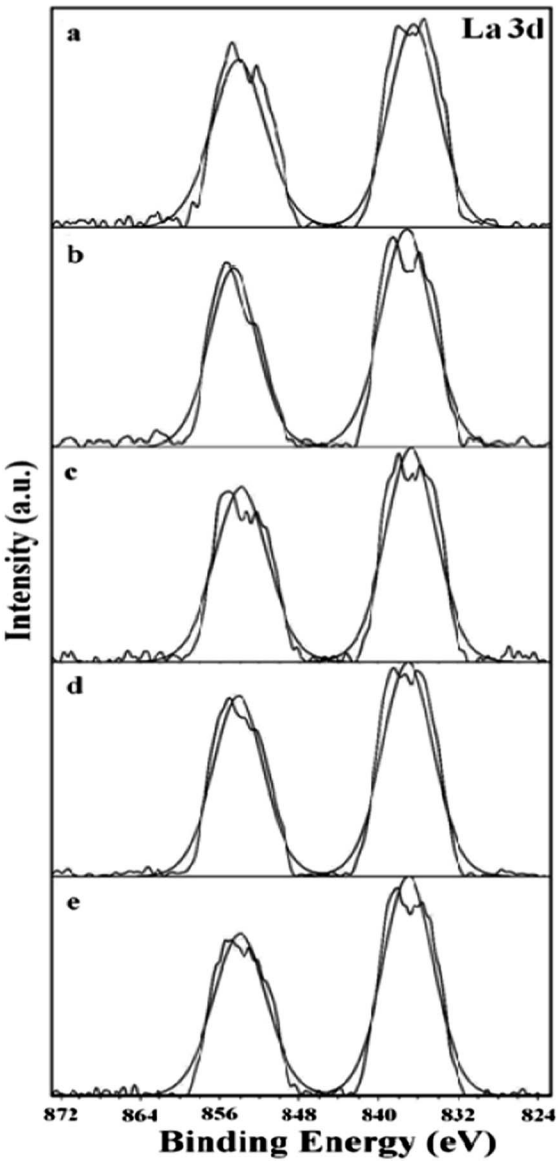

Fig. 3 La 3d core level XPS spectra of La–Ni_x–Ce_{1-x} mixed oxide catalysts. (a) $x = 1$; (b) $x = 0.6$; (c) $x = 0.4$; (d) $x = 0.3$; (e) $x = 0.2$.

The Ce 3d XP spectra of $LaNi_xCe_{1-x}$ catalysts are shown in Fig. 4. As can be seen from the figure, the Ce 3d XP spectra are complex and appear in the range of 880–920 eV due to the hybridization of the O 2p valence band with the Ce 4f level in the final state of photoionization.[23,24] The Ce $3d_{5/2}$ peaks appear to be more intense in comparison to Ce $3d_{3/2}$ peaks, suggesting that cerium exists mainly in Ce^{4+} oxidation state.

On the other hand, the stabilization of certain amount of Ce^{3+} oxidation state is also observed in samples with low Ce-content, where the intensity of the satellite peak around 916.6 eV decreases with simultaneous increase in the characteristic peaks of Ce^{3+} (885.7 and 903.9 eV). These results suggest that at low concentrations of Ce ($x = 0.8$, 0.6 and 0.4) it exists as Ce^{3+} ion, whereas the excess cerium in higher concentrations exists as Ce^{4+}. These results evidently support the observations made

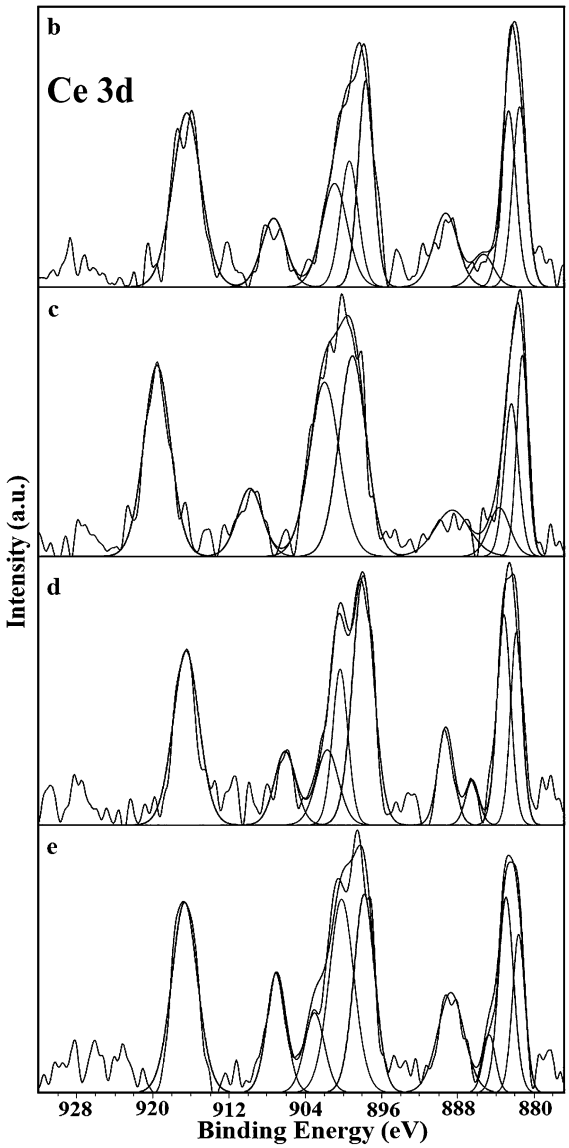

Fig. 4 Ce 3d core level spectra of La–Ni_x–Ce_{1-x} mixed oxide catalysts. (a) $x = 0.6$; (b) $x = 0.4$; (c) $x = 0.3$; and (d) $x = 0.2$.

from the TPR and XRD analyses, where the Ce–Ni interaction prevails in the low Ni containing catalysts.

Two O 1s peaks are noticed in the ranges 529.2–531.9 eV and 529.9–532.3 eV for all samples which can be attributed to presence of hydroxyl and carbonate groups and adsorbed water (Fig. S3, ESI†).[25] The obtained C 1s spectra show two main peaks at ~284.6 and 285.9 eV which might be due to hydrocarbon contamination (C–C/C–H and C–O bonds) (Fig. S4, ESI†). Besides, the small peak observed in the region of 288.9–289.3 eV represents the carbonate species[25,26] which reacted with La^{3+} when exposed to atmosphere.

A comparison of the XPS data of the sol–gel catalysts, with those prepared by the hydrothermal method reveals that when $x = 0.2$ and 0.3, the hydrothermal catalysts have their XPS peaks with B.E. at 855.3 eV, about 2 eV higher than those of the corresponding sol–gel catalysts. The higher B.E. of Ni represents its +3 state, possibly the Ni existing in the $LaNiO_3$ perovskite form. The lower B.E. of 853.7 eV for the sol–gel catalysts suggests that the Ni exists in its +2 state.

3.4 Fourier transform infrared spectroscopy

The results of characterization performed using FT-IR spectroscopy are shown in Fig. 5. With the usage of nitrate precursors in catalyst preparation, the residual nitrates can be present in the coordination sphere of the corresponding metallic cation, in turn surrounded by a propionic acid molecule (bands at ~853, 1379 and 1464–1471 cm^{-1}). The observed IR band in the range of 3000–3600 cm^{-1} correspond to –OH stretching of structural hydroxyl groups and physisorbed and interlayer water.[26,27] The IR spectrum of $LaNiO_3$ catalyst does not show any characteristic peaks due to its low resistivity.[28,29] All catalysts show bands in the region of 546–489 cm^{-1}, in agreement with the vibrational stretching frequencies of the metal–oxygen bonds.[15,30]

3.5 Catalytic activity test

The activity of the La–Ni_x–Ce_{1-x} mixed oxide catalysts during the methane dry reforming was evaluated at 800 °C and atmospheric pressure. It can be observed that the activity of the La–Ni_x–Ce_{1-x} catalysts increases upto $x = 0.4$ and then on decreases continuously. $LaNi_{0.4}Ce_{0.6}O_3$ has exhibited the highest activity among all the catalysts reaching the conversion levels of more than 90%. The $LaNiO_3$ has shown low conversions (less than 20%) for both methane and carbon dioxide under the conditions of evaluation. This interesting observation clearly suggests the significance of the Ce in the dry reforming of methane. The initial increase in the conversions of methane and carbon dioxide can be attributed to the availability of well dispersed nickel. Fig. 6 reveals the variations in dispersion and also catalytic activity with the change in Ni content. The

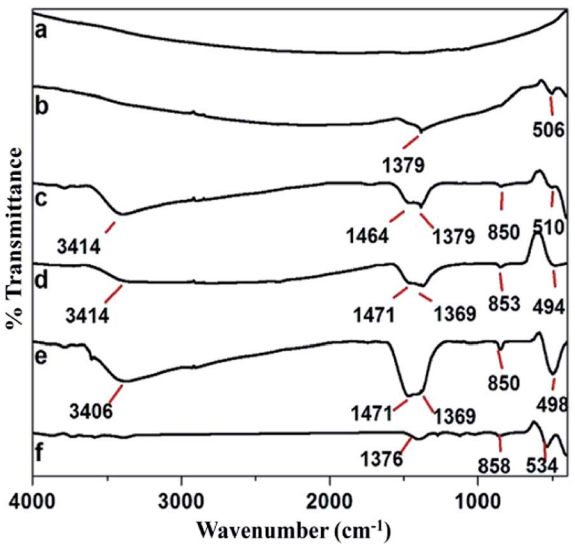

Fig. 5 FT-IR patterns of La–Ni_x–Ce_{1-x} mixed oxide catalysts. (a) $x = 1$; (b) $x = 0.8$; (c) $x = 0.6$; (d) $x = 0.4$; (e) $x = 0.3$; and (f) $x = 0.2$.

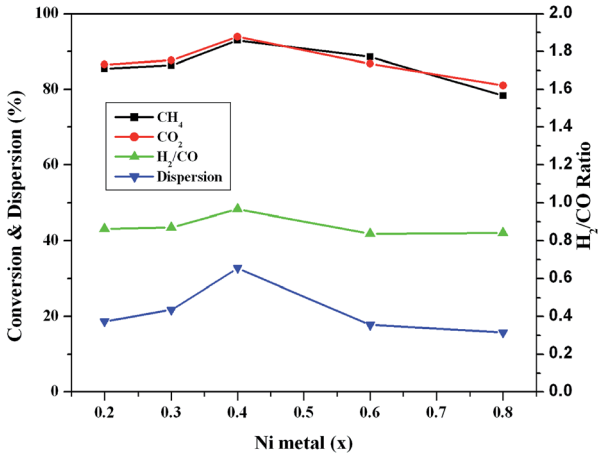

Fig. 6 Variation of activity and Ni dispersion with x, in the La–Ni_x–Ce_{1-x} mixed oxide ($0 < x < 1$) sol–gel catalysts.

dispersion and activity curves varied in a similar fashion, implying that activity is proportional to dispersion. The high activity of catalysts even at low x values can be understood as a result of higher dispersion. The hydrothermally prepared catalysts, reported in our previous publication showed low dispersion as described above. The decrease in conversions could be a result of Ni agglomeration.

It is a well-established fact in the literature that Ni^0 is the active site for dry reforming of methane.[8,31] $LaNiO_3$ ultimately leads to the formation of well-dispersed Ni on La_2O_3. When Ce is substituted for La, Lima *et al.*[18] reported the possibility of formation of Ni/La–Ce–O. By keeping La constant and varying Ce and Ni content, in the present catalysts, we propose that apart from the formation of the perovskite, the additional nickel existed in a well dispersed form. At low values of x the formation of Ni–Ce oxide solid solution appears to be feasible. As the x value increases its composition decreases. In the case of $LaNi_{0.4}Ce_{0.6}O_3$ the active Ni species might have reached its optimum level, making it the best catalyst. The existence of CeO_2 in the proximity of Ni helps in further increasing the activity.[32,33] It was reported that the formation of Ni–Ce solid solution improves the stability of the catalysts by modifying the chemical environment around Ni.[17] CeO_2 is reduced either by the hydrogen formed during the reaction or by the carbon deposits formed during the decomposition of methane on Ni sites. CO_2 is decomposed on reduced ceria (Ce_2O_3), in turn oxidizing it to CeO_2 and forming CO. Thus, the variation of Ce–Ni ratio in La–Ce–Ni mixed oxide (rather than La–Ce ratio) appears to have a positive effect in getting higher conversions (more than 90% for both the gases). Therefore, the superior catalytic performance of the $LaNi_{0.4}Ce_{0.6}O_3$ can be explained by the formation of highly dispersed Ni on CeO_2 or La_2O_3 or their mixed oxide, as proposed by Lima *et al.*, The formation of Ni–Ce solid solution stabilizes the dispersed Ni. The higher conversion of CO_2 might be due to the facile reverse water gas shift reaction, as reported previously.[34]

The results of time-on-stream analysis performed on $LaNi_{0.4}Ce_{0.6}O_3$ catalyst are shown in Fig. 7. Promising conversions for both methane (91.6%) and carbon dioxide (93.5%) can be observed. The catalyst also retained its activity to a larger extent during the 9 h on time, showing a reasonable stability. Similarly, the syngas ratio also attained a steady value in the region of 0.87–0.84.

A comparison of the XRD results of the sol–gel catalysts before and after reaction reveals that there is a decrease in the intensity of $LaNiO_3$ signal in the used catalysts (Fig. S5, ESI†). This may be due to the reduction of catalysts in hydrogen flow prior to the activity run. The catalysts showed sintering tendency, though not severe. This is observed by the H_2 chemisorptions studies of the fresh and used ($x = 0.4$) catalysts where only a slight increase in the particle size from 32.1 to 38.5 Å is recorded.

Table 3 presents the coke content of the catalysts measured after 9 h of evaluation. In all the cases the sol–gel catalysts recorded lower values, than the corresponding hydrothermally prepared catalysts. Thus, the sol–gel catalysts are found to be less susceptible to coking.

A comparison of the activity patterns of the $LaNi_{0.4}Ce_{0.6}O_3$ sol–gel and hydrothermally prepared catalysts is shown in Fig. 8. Over a period of 9 h, the sol–gel catalyst has exhibited higher conversions of both CO_2 and CH_4 revealing its superiority.

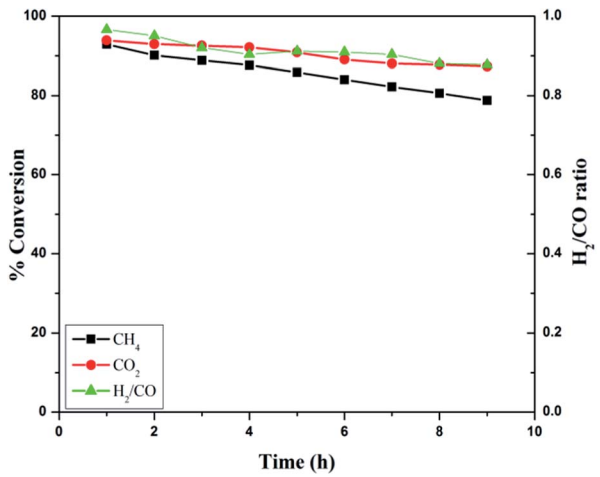

Fig. 7 Time on stream behaviour of $LaNi_{0.4}Ce_{0.6}O_3$ catalyst during the dry reforming of methane at 800 °C.

Table 3 Coke content of the catalysts measured after 9 h of evaluation

	Carbon (%)	
Catalyst	Sol–gel	Hydrothermal
$LaNi_{0.8}Ce_{0.2}O_3$	0.34	0.55
$LaNi_{0.6}Ce_{0.4}O_3$	0.18	0.39
$LaNi_{0.4}Ce_{0.6}O_3$	0.15	0.34
$LaNi_{0.3}Ce_{0.7}O_3$	0.2	0.38
$LaNi_{0.2}Ce_{0.8}O_3$	0.25	0.32

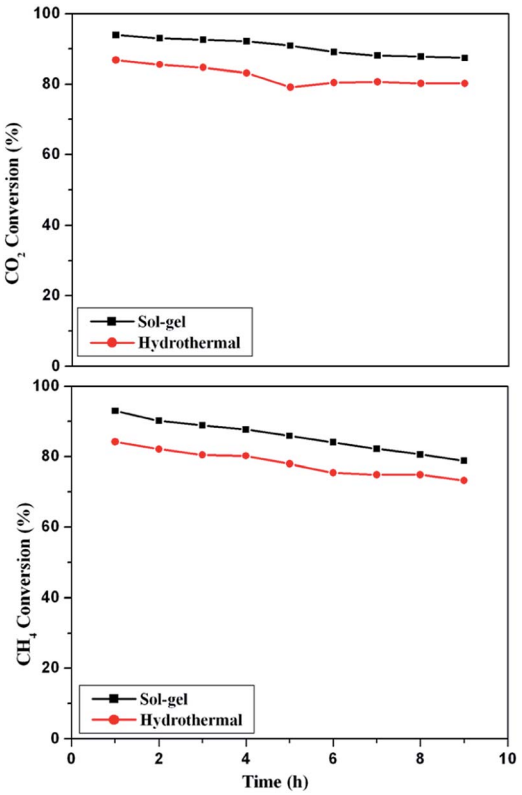

Fig. 8 A comparison of the activity profiles of the $LaNi_{0.4}Ce_{0.6}O_3$ sol–gel and hydrothermal catalysts.

4. Conclusions

The sol–gel method of preparation of the catalysts is found to be advantageous than the hydrothermal method, in terms of higher activity even at lower Ni compositions. The catalysts exhibit high surface areas, possess better Ni dispersion and are less susceptible to coking. $LaNi_{0.4}Ce_{0.6}O_3$ catalyst shows the maximum activity. It shows reasonable stability during the reaction.

Acknowledgements

The authors thank Council of Scientific and Industrial Research (CSIR), New Delhi for the financial support.

References

1 R. Burch and M. I. Petch, *Appl. Catal., A*, 1992, **88**, 39.
2 F. Solymosi, G. Kutsan and A. Erdöhelyi, *Catal. Lett.*, 1991, **11**, 149.
3 P. M. Torniainen, X. Chu and L. D. Schmidt, *J. Catal.*, 1994, **146**, 1.
4 S. C. Tsang, J. B. Claridge and M. L. H. Green, *Catal. Today*, 1995, **23**, 3.
5 J. R. Rostrup-Nielsen, in *Catal. Sci. Technol.*, ed. J. R.Anderson and M.Boudart, Springer Publishing, Berlin, 1984, vol. 5, pp. 1–117.
6 J. R. Mawdsley and T. R. Krause, *Appl. Catal., A*, 2008, **334**, 311.
7 G. R. Moradi, F. Khosravian and M. Rahmanzadeh, *Chin. J. Catal.*, 2012, **33**, 797.
8 P. Moradi and M. Parvari, *Iran. J. Chem. Eng.*, 2006, **3**, 29.
9 H. Provendier, C. Petit, J. L. Schmitt, A. Kienneman and C. Chaumont, *J. Mater. Sci.*, 1999, **34**, 4121.
10 N. Laosiripojana and S. Assabumrungrat, *Appl. Catal., B*, 2005, **60**, 107.
11 W. Dong, K. Jun, H. Roh, Z. Liu and S. Park, *Catal. Lett.*, 2002, **78**, 215.
12 L. Pino, V. Recupero, S. Beninati, A. K. Shukla, M. S. Hedge and P. Bera, *Appl. Catal., A*, 2002, **225**, 63.
13 A. Nandini, K. K. Pant and S. C. Dhingra, *Appl. Catal., A*, 2005, **290**, 166.
14 A. Qi, S. Wang, G. Fu, C. Ni and D. Wu, *Appl. Catal., A*, 2005, **281**, 233.
15 T. V. Sagar, N. Sreelatha, G. Hanmant, K. Upendar, N. Lingaiah, K. S. Rama Rao, C. V. V. Satyanarayana, I. A. K. Reddy and P. S. Sai Prasad, *Indian J. Chem., Sect. A: Inorg., Bio-inorg., Phys., Theor. Anal. Chem.*, 2014, **53**, 478.
16 A. S. Larimi and S. M. Alavi, *Int. J. Chem. Eng. Appl.*, 2012, **3**, 6.
17 S. Xu, X. Yan and X. Wang, *Fuel*, 2006, **85**, 2243.
18 S. M. Lima, J. M. Assaf, M. A. Peña and J. L. G. Fierro, *Appl. Catal., A*, 2006, **311**, 94.
19 C. Pirez, M. Capron, H. Jobic, F. Dumeignil and L. Jalowiecki-Duhamel, *Angew. Chem., Int. Ed.*, 2011, **50**, 10193.
20 W. Yonggang, W. Hua, L. Kongzhai, Z. Xing and D. Yunpeng, *J. Rare Earths*, 2010, **28**, 357.
21 L. P. Haack, C. R. Peters, J. E. Vriesand and K. Otto, *Appl. Catal., A*, 1992, **87**, 103.
22 M. A. Kumar, Ch. Venumadhav, T. V. Sagar, M. Surendar, N. Lingaiah, G. N. Rao and P. S. Sai Prasad, *Indian J. Chem., Sect. A: Inorg., Bio-inorg., Phys., Theor. Anal. Chem.*, 2014, **53**, 530.
23 P. Sudarsanam, B. Mallesham, P. S. Reddy, D. Großmann, W. Grünert and B. M. Reddy, *Appl. Catal., B*, 2014, **144**, 900.
24 K. Kuntaiah, P. Sudarsanam, B. M. Reddy and A. Vinu, *RSC Adv.*, 2013, **3**, 7953.
25 J. L. G. Fierro, *Catal. Today*, 1990, **8**, 153.
26 M. A. Peña and J. L. G. Fierro, *Chem. Rev.*, 2001, **101**, 1981.
27 C. E. Daza, J. Gallego, J. A. Moreno, F. Mondragón, S. Moreno and R. Molina, *Catal. Today*, 2008, **133–135**, 357.
28 P. Ganguly and N. Y. Vasanthacharya, *J. Solid State Chem.*, 1986, **61**, 164.
29 T. Vaz and A. V. Salker, *Mater. Sci. Eng., B*, 2007, **143**, 81.
30 R. A. Nyquist, C. L. Putzig and M. A. Leugers, in *The Handbook of Infrared and Raman spectra of Inorganic Compounds and Organic Salts*, ed. A. R. Nyquist, C. L. Putzig and M. A. Leugers, Academic Press Ltd., San Diego, CA, 1997, vol. 4.
31 A. Khalesi, H. R. Arandiyan and M. Parvari, *Chin. J. Catal.*, 2008, **29**, 960.
32 J. A. Montoya, E. Romero-Pascual, C. Gimon, P. Del Angel and A. Monzón, *Catal. Today*, 2000, **63**, 71.
33 N. Laosiripojana, W. Sutthisripok and S. Assabumrungrat, *Chem. Eng. J.*, 2005, **112**, 13.
34 U. H. Taufiq-Yap, U. S. Rashid and Z. Zainal, *Appl. Catal., A*, 2013, **468**, 359.

